

Three-state coherent control using narrowband and passband sequences

Cheng Zhang, Li-Tuo Shen, Yan Xia, and Zhi-Cheng Shi*

Fujian Key Laboratory of Quantum Information and Quantum Optics,

Fuzhou University, Fuzhou 350108, China and

Department of Physics, Fuzhou University, Fuzhou 350108, China

Jie Song

Department of Physics, Harbin Institute of Technology, Harbin 150001, China

In this work, we propose a comprehensive design for narrowband and passband composite pulse sequences by involving the dynamics of all states in the three-state system. The design is quite universal as all pulse parameters can be freely employed to modify the coefficients of error terms. Two modulation techniques, the strength and phase modulations, are used to achieve arbitrary population transfer with a desired excitation profile, while the system keeps minimal leakage to the third state. Furthermore, the current sequences are capable of tolerating inaccurate waveforms, detunings errors, and work well when rotating wave approximation is not strictly justified. Therefore, this work provides versatile adaptability for shaping various excitation profiles in both narrowband and passband sequences.

I. INTRODUCTION

In recent decades, the composite pulse (CP) technique [1–5] has gained widespread attraction in quantum information processing [6–8]. This technique was originally developed in fields of polarization optics [9] and nuclear magnetic resonance (NMR) [10–14]. Since then, it has been utilized in various branches of physics [15–25] with a particular focus on quantum control [26–32]. The CP sequence, a series of constant pulses with appropriate relative phases, has reliably accomplished several desired quantum tasks and efficiently compensated

*szc20147@163.com

errors caused by external noises [33–37]. A well-known one is the broadband sequence [38–42], which is widely adopted to improve the error-resistant ability for the implementation of single- and multi-qubit quantum gates [43–51]. However, it is not a panacea and sometimes unsuitable for some specific tasks, such as addressing operations in trapped ions [52] and optical lattice systems [53–55]. On these occasions, the narrowband (NB) sequence [56–61] offers a more suitable candidate.

The NB sequence aims at enhancing sensitivity to systematic errors. More specifically, system states are allowed to evolve only within a specific error threshold, and their evolutions are inhibited when falling below this threshold [60]. In essence, the system states remain unchanged once the parameter deviates significantly from the precise value [62]. This unique feature makes the NB sequence perfectly adaptive to local addressing operations in quantum computation [57], because the excitation of the particles surrounding the object can be efficiently inhibited. Additionally, in order to enhance the resilience of this addressing operation against minor systematic errors, the passband (PB) sequence was developed [62–66]. The versatility of the PB sequence is demonstrated in two primary ways: it can successfully correct small errors in parameters, and significantly prohibit the system evolution when the errors are large enough [63]. Recently, the NB sequence has proven to be a valuable aid in spatial localization for biological or medical NMR spectroscopy [56], while the PB sequence has emerged as an efficient tool for selecting high-intensity target signals and suppressing unwanted background signals in NMR experiments [67].

So far, the researches on NB and PB sequences [56–65] have primarily focused on two-state systems. When performing individual addressing operations on a three-state system, the sequences derived from two-state systems cannot be directly applied due to their different structures. Moreover, there is only one coupling strength in the two-state system while it has two coupling strengths in the three-state system. This trait allows one to adjust the ratio of the two coupling strengths to design broadband sequences in the three-state system [42]. Another significant difference is the participation of the third state in the system evolution. In a two-state system, only the population of one state needs to be calculated, because the other state is naturally obtained according to the normalization condition. In contrast, if there is leakage to the third state, population transfer would be incomplete, leading to imperfect quantum control in a three-level system.

In previous work [49], with the help of the Morris-Shore transformation [68] and Majorana

decomposition [69], the three-state system can be reduced into an effective two-state one. As a result, it is impossible to consider the dynamics of the excited state, completely neglecting population leakage to the excited state. In the presence of leakage, the well-designed CP sequences [62] may be invalid in three-state systems. Hence, it is necessary to contain the dynamics of all system states for NB and PB sequences. On the other hand, predetermining physical parameters (except for the modulation parameters) may fail to fully nullify derivatives, ultimately jeopardizing the construction of NB and PB sequences in the three-state system. Therefore, a general method needs to be developed for constructing NB and PB sequences applied to various types of modulations in three-state systems.

In this paper, we construct the NB and PB sequences for arbitrary population transfer in the three-state system. The design procedure entails modifying the error coefficients in the transition probability, thereby identifying appropriate modulation parameters for the NB and PB sequences. When the error coefficients cannot be completely nullified, we propose a cost function to obtain a suitable substituted solution that minimizes the coefficients as much as possible. Two modulation techniques, the strength and phase modulations, are employed for creating the NB sequences with almost identical shapes of the excitation profile, as well as the PB sequences with a desired excitation profile. Furthermore, both NB and PB sequences exhibit significant reduction in leakage to the third state. The numerical results indicate that the strength modulation has adaptability to inaccurate waveforms, while the phase modulation shows resistance to detuning errors. Besides, both modulations show resistance to the case that the rotating wave approximation (RWA) is not strictly justified.

This paper is organized as follows. In Sec. II, we introduce the physical model and propose the general design method for NB and PB sequences in the three-state system. In Sec. III, we illustrate how to construct the NB and PB sequences with specific pulse numbers by the strength and phase modulations. For each modulation, the sequences up to seven pulses are investigated. In Sec. IV, we take five pulses to exemplify the construction of the NB and PB sequences for arbitrary population transfer between two lower states. In Sec. V, we demonstrate the validity of the current sequences when the pulse is imperfect. The conclusion is given in Sec. VI.

II. PHYSICAL MODEL AND GENERAL THEORY

Let us consider a paradigmatic three-state system with the Λ -type structure, as shown in Fig. 1(a). The transition frequency between the lower state $|g\rangle(|f\rangle)$ and the excited state $|e\rangle$ is $\omega_{g(f)} = [E_e - E_{g(f)}] / \hbar$ with level energy $E_k (k = g, f, e)$. Here, two lower states are forbidden for direct transition and coupled to the excited state by two control fields $\Omega(t) = \Omega \cos(\omega'_g t + \phi)$ and $\lambda(t) = \lambda \cos(\omega'_f t + \varphi)$ with frequencies ω'_g and ω'_f , coupling strengths Ω and λ , and phases ϕ and φ , respectively. The Hamiltonian of the system reads ($\hbar = 1$ hereafter)

$$H = \sum_{k=g,f,e} E_k |k\rangle \langle k| + \Omega \cos(\omega'_g t + \phi) |g\rangle \langle e| + \lambda \cos(\omega'_f t + \varphi) |f\rangle \langle e| + \text{H.c.} \quad (1)$$

In the rotating frame $R = |g\rangle \langle g| + \exp(i\omega'_f t) |f\rangle \langle f| + \exp(i\omega'_g t) |e\rangle \langle e|$, the Hamiltonian under RWA can be rewritten as

$$H = \frac{\Omega}{2} e^{i\phi} |g\rangle \langle e| + \frac{\lambda}{2} e^{i\varphi} |f\rangle \langle e| + \text{H.c.}, \quad (2)$$

where we assume $\delta_g = \omega_g - \omega'_g = 0$ and $\delta_f = \omega_f - \omega'_f = 0$ for simplicity, as shown in Fig. 1(b). Note that the RWA is well satisfied in the atomic system driven by laser fields, where the coupling strength $\Omega(\lambda)$ can be varied via manually controlling the intensity of laser fields, while the phase $\phi(\varphi)$ can be regulated by adjusting the phase of laser fields [70–73] via an electro-optical or acousto-optical modulator [63].

When the Hamiltonian (2) is time-independent, the propagator at the evolution time T reads $U(T) = \exp(-iHT)$. It is instructive to adopt its matrix form in the basis $\{|g\rangle, |f\rangle, |e\rangle\}$

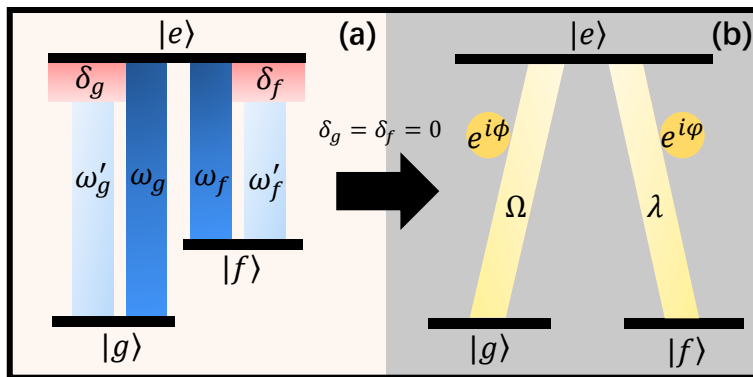


FIG. 1: A Λ -type three-state system driven by two control fields (a) in the original picture and (b) in the rotating frame.

up to a global phase

$$U = \begin{bmatrix} \cos^2 \theta + \cos \frac{A}{2} \sin^2 \theta & \sin^2 \frac{A}{4} \sin 2\theta e^{i(\phi-\varphi)} & -i \sin \frac{A}{2} \sin \theta e^{i\phi} \\ \sin^2 \frac{A}{4} \sin 2\theta e^{i(\varphi-\phi)} & \sin^2 \theta + \cos \frac{A}{2} \cos^2 \theta & -i \sin \frac{A}{2} \cos \theta e^{i\varphi} \\ -i \sin \frac{A}{2} \sin \theta e^{-i\phi} & -i \sin \frac{A}{2} \cos \theta e^{-i\varphi} & \cos \frac{A}{2} \end{bmatrix}, \quad (3)$$

where $A = \Omega_0 T$ is the pulse area. We define $\Omega = \Omega_0 \sin \theta$ and $\lambda = \Omega_0 \cos \theta$, and thus $\tan \theta = \Omega/\lambda$, where θ is called the coupling strength ratio.

The propagator of the N -pulse sequence is yielded by a product of the propagators of single resonant pulses, i.e.,

$$U^{(N)}(NT) = U_N U_{N-1} \cdots U_2 U_1, \quad (4)$$

where U_n represent the evolution operator of the n^{th} pulse, $n = 1, 2, \dots, N$. Obviously, the total propagator depends on all modulation parameters of the ingredient pulses, labeled as $\{A_n, \theta_n, \phi_n, \varphi_n\}$.

Assume that each pulse has identical pulse area 2π and the same pulse area error ϵ , i.e., the actual pulse area for each pulse reads $A_n = 2\pi(1 + \epsilon)$. According to the definition of the pulse area, the error ϵ refers to either the coupling strength error $\Omega_0(1 + \epsilon)$ or the pulse duration error $T(1 + \epsilon)$ under the resonance condition. In this way, the transition probability of the state $|f\rangle$ can be labelled as $P_f^{(N)}(\boldsymbol{\theta}, \boldsymbol{\phi}, \boldsymbol{\varphi}, \epsilon)$, where $\boldsymbol{\theta} = (\theta_1, \dots, \theta_N)$, $\boldsymbol{\phi} = (\phi_1, \dots, \phi_N)$ and $\boldsymbol{\varphi} = (\varphi_1, \dots, \varphi_N)$. The primary objective is to implement population transfer between the states $|g\rangle$ and $|f\rangle$ in a desired manner. Namely, the transition probability of the target state satisfies

$$P_f^{(N)}(\boldsymbol{\theta}, \boldsymbol{\phi}, \boldsymbol{\varphi}, 0) = \mathcal{P}, \quad (5)$$

where \mathcal{P} is a predetermined value. Remarkably, complete population inversion is achieved by setting $\mathcal{P} = 1$.

Generally speaking, for the NB sequence, the transition probability must drop sharply around the target pulse area $A_n = 2\pi$ and be ‘‘frozen’’ around $A_n = 4\pi$ in the excitation profile. The physical effect of this setting is that quantum operations are extremely sensitive to errors, so that one can achieve precise addressing control in dispersion external fields. Mathematically, the excitation profile for the NB sequence is acquired via nullifying the derivatives of $P_f^{(N)}(\boldsymbol{\theta}, \boldsymbol{\phi}, \boldsymbol{\varphi}, \epsilon)$ at $\epsilon = \pm 1$ in order. We can seek the modulation parameters

of the NB sequence, i.e., $\boldsymbol{\theta}$, $\boldsymbol{\phi}$ and $\boldsymbol{\varphi}$, through fulfilling a group of equations on the derivatives

$$\tilde{x}_{N,m}(\boldsymbol{\theta}, \boldsymbol{\phi}, \boldsymbol{\varphi}) = \frac{1}{m!} \frac{\partial^m}{\partial \epsilon^m} \left[P_f^{(N)}(\boldsymbol{\theta}, \boldsymbol{\phi}, \boldsymbol{\varphi}, \epsilon) \right] \Big|_{\epsilon=\pm 1} = 0, \quad (6)$$

where $\tilde{x}_{N,m}(\boldsymbol{\theta}, \boldsymbol{\phi}, \boldsymbol{\varphi})$ is the coefficient of the m^{th} order error term in the Taylor expansion at $\epsilon = \pm 1$, and $m = 4, 6, \dots, M_N$. Note that $\tilde{x}_{N,2}$ and all odd-order coefficients naturally vanish due to the choice of $A_n = 2\pi$.

For the PB sequence, the transition probability needs to maintain unchanged around $A_n = 2\pi$ meanwhile vanish around $A_n = 4\pi$. To this end, we have to nullify the error terms in the transition probability at both $\epsilon = 0$ and $\epsilon = \pm 1$, and thus the modulation parameters are obtained by solving the following equations

$$\begin{cases} \tilde{x}_{N,m}(\boldsymbol{\theta}, \boldsymbol{\phi}, \boldsymbol{\varphi}) = \frac{1}{m!} \frac{\partial^m}{\partial \epsilon^m} \left[P_f^{(N)}(\boldsymbol{\theta}, \boldsymbol{\phi}, \boldsymbol{\varphi}, \epsilon) \right] \Big|_{\epsilon=\pm 1} = 0, \\ x_{N,m'}(\boldsymbol{\theta}, \boldsymbol{\phi}, \boldsymbol{\varphi}) = \frac{1}{m'!} \frac{\partial^{m'}}{\partial \epsilon^{m'}} \left[P_f^{(N)}(\boldsymbol{\theta}, \boldsymbol{\phi}, \boldsymbol{\varphi}, \epsilon) \right] \Big|_{\epsilon=0} = 0, \end{cases} \quad (7)$$

where $x_{N,m'}(\boldsymbol{\theta}, \boldsymbol{\phi}, \boldsymbol{\varphi})$ is the coefficient of the m'^{th} order error term in the Taylor expansion at $\epsilon = 0$, $m = 4, 6, \dots, M_P$, and $m' = 2, 4, \dots, M'_P$. From the view of the physical picture, the excitation profile exhibits narrow wings with a large M_P , while its central flat top becomes wider as M'_P increases. Without causing ambiguity, we omit the symbol $(\boldsymbol{\theta}, \boldsymbol{\phi}, \boldsymbol{\varphi})$ in expressions hereafter.

It is worth noting that the above design method may not succeed, since either Eqs. (6) or (7) sometimes are unsolvable. On this occasion, we can identify a substituted group of solutions to significantly reduce low-order error coefficients. The substituted solution can be obtained by minimizing a cost function established by Eqs. (7), which has different forms for the NB and PB sequences:

$$\text{Narrowband : } \mathcal{F}_{\text{NB}}^{(N)} = \sum_{m=4}^{M_N} c_m |\tilde{x}_{N,m}|, \quad (8a)$$

$$\text{Passband : } \mathcal{F}_{\text{PB}}^{(N)} = \sum_{m=4}^{M_P} c_m |\tilde{x}_{N,m}| + \sum_{m'=2}^{M'_P} c'_m |x_{N,m'}|, \quad (8b)$$

where $c_{m(m')}$ is the weight factor. To ensure that the cost function gives more weight to low-order error coefficients and alleviate the contribution of high-order ones, the weight factor should decrease monotonously with an increase in $m(m')$.

Alternatively, by setting $0 < \mathcal{P} < 1$, the current method is also feasible to construct the NB and PB sequences for arbitrary population transfer between two lower states in the

three-state system. Unlike two-state systems [74, 75], we have to consider the evolution of the third state, and the leakage to the third state must be suppressed to restrict the system dynamics within two states $\{|g\rangle, |f\rangle\}$. Hence, apart from satisfying Eqs. (5)-(7), the modulation parameters of NB and PB sequences should meet the following equations

$$\begin{cases} \tilde{y}_{N,l} = \frac{1}{l!} \frac{\partial^l}{\partial \epsilon^l} [P_e^{(N)}(\epsilon)] \Big|_{\epsilon=\pm 1} = 0, \\ y_{N,l'} = \frac{1}{l'!} \frac{\partial^{l'}}{\partial \epsilon^{l'}} [P_e^{(N)}(\epsilon)] \Big|_{\epsilon=0} = 0, \end{cases} \quad (9)$$

where $P_e^{(N)}(\epsilon)$ is the transition probability of the third state $|e\rangle$, $l = 2, 4, \dots, L$, and $l' = 2, 4, \dots, L'$. Again, $y_{N,0}$, $\tilde{y}_{N,0}$, and all odd-order coefficients in Eq. (9) vanish by setting $A_n = 2\pi$. Next, we elucidate the CP design in detail by exemplifying specific pulse numbers.

III. PULSE SEQUENCE DESIGN

In this section, we demonstrate how to design various kinds of CP sequences in the three-state system. Two modulation techniques, the strength and phase modulations, are adopted in the design procedure. For a certain modulation, all parameters are fixed except for the modulation one.

A. Strength modulation

We first elaborate on the construction of NB and PB sequences by the strength modulation. For brevity, the N -pulse NB and PB sequences by the strength modulation are called as the S-NBN and S-PBN sequences, respectively. The phase differences in each pulse are held on constant, e.g., $\phi_n = \pi/2$ and $\varphi_n = 0$ with $n = 1, 2, \dots, N$. Noting that there are two coupling strengths Ω_n and λ_n for the n^{th} pulse, we label the coupling strength ratio as $\tan \theta_n = \Omega_n/\lambda_n$, and θ_n are recognized as the modulation parameters. Physically, we can modulate one of two coupling strengths while fixing another to obtain the variables θ_n .

The target propagator of the N -pulse sequence in the absence of errors is

$$U^{(N)} = \begin{bmatrix} \cos \tilde{\theta}_N & -i \sin \tilde{\theta}_N & 0 \\ i^{(2N+3)} \sin \tilde{\theta}_N & (-1)^N \cos \tilde{\theta}_N & 0 \\ 0 & 0 & (-1)^N \end{bmatrix}, \quad (10)$$

where $\tilde{\theta}_N = 2 \sum_{n=1}^N (-1)^{n+1} \theta_n$. Obviously, to ensure complete population inversion, the strength ratio of the first pulse can be chosen as

$$\theta_1 = \sum_{n=2}^N (-1)^n \theta_n + \frac{(2k+1)\pi}{4}, \quad (11)$$

where k is an arbitrary integer. Through this selection, we have

$$\tilde{\theta}_N = \frac{\pi}{2} + 2k\pi. \quad (12)$$

Then, the remaining $(N-1)$ ratios are obtained by solving Eqs. (6) for the S-NBN sequence or Eqs. (7) for the S-PBN sequence.

For examples, to construct the S-NB2 sequence for complete population inversion between $|g\rangle \leftrightarrow |f\rangle$, we need to solve Eqs. (5) and (6) with $M_N = 4$, i.e.,

$$x_{2,0} = \sin^2 2(\theta_1 - \theta_2) = 1, \quad (13a)$$

$$\tilde{x}_{2,4} = \frac{\pi^4}{4} [\sin \theta_1 \cos \theta_1 + \cos \theta_2 (2 \sin \theta_1 + \sin \theta_2)]^2 = 0, \quad (13b)$$

and one group solution for θ_1 and θ_2 are ($k=0$)

$$\theta_1 = \theta_2 + \frac{\pi}{4}, \quad \theta_2 = \frac{5\pi}{8} - \frac{1}{2} \arctan \sqrt{2(1+\sqrt{2})}. \quad (14)$$

As for the design of S-NB3 sequence, all θ_n are derived in a similar way, through setting $M_N = 6$, and the numerical solutions are given in Table I. We can continue to combine more pulses for longer NB sequences. Figure 2(a) displays the excitation profiles for the single pulse and the S-NBN sequences from $N=2$ to $N=7$, respectively. Apparently, with the pulse number N increasing, the excitation profile becomes narrower.

In order to quantitatively measure the magnitude of the efficient excitation region, we define the low excitation width W_l to represent the bilateral low excitation region, i.e.,

$$W_l = W_{\text{right}} + W_{\text{left}} = |1 - \epsilon_l^+| + |1 + \epsilon_l^-|, \quad (15)$$

where $W_{\text{right(left)}}$ denotes the width of the low excitation region on right (left) side, and ϵ_l^+ and ϵ_l^- are two solutions for the transition probability satisfying $P_f^{(N)}(\epsilon) = 10^{-4}$. As shown in Fig. 2(b), W_l gradually enlarges with the increasing of the pulse number. In particular, the S-NBN sequence with few pulses (e.g., $N=2$ or $N=3$) can significantly compress the excitation region, leading to a remarkable improvement of the sensitivity around $\epsilon=0$. For

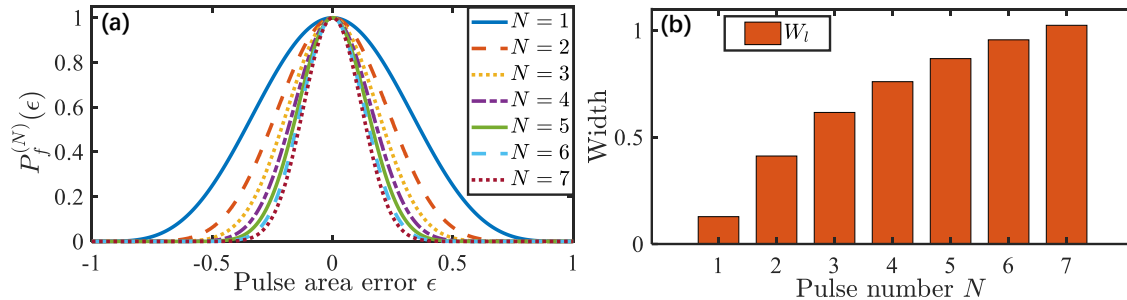


FIG. 2: (a) Excitation profiles for the S-NBN sequences. (b) Low excitation width W_l vs the pulse number N in the S-NBN sequences. For $N = 1$, $\theta_1 = \pi/4$ and $\phi_1 = \varphi_1 = 0$. All θ_n come from Table I.

TABLE I: Coupling strength ratios θ_n for the S-NBN sequences (in units of π).

	θ_1	θ_2	θ_3	θ_4	θ_5	θ_6	θ_7
S-NB2	0.6930	0.4430	–	–	–	–	–
S-NB3	0.9223	0.9908	0.3185	–	–	–	–
S-NB4	1.8111	0.3617	1.7659	0.9653	–	–	–
S-NB5	0.8578	0.3304	1.4755	1.3296	1.5767	–	–
S-NB6	1.1688	1.7614	0.5511	0.3724	1.5905	0.9266	–
S-NB7	0.7487	1.9199	1.2087	1.5952	0.3258	0.8483	0.3301

the S-NB7 sequence, the excitation profile has a wide range of the low excitation on both sides ($W_l = 1.022$).

Note that we are unable to obtain the excitation profile for the S-PB2 sequence, because three subequations in Eqs. (5) and (7) cannot be simultaneously satisfied by only two modulation parameters. To construct the S-PB3 sequence, we set $M_P = 4$ and $M'_P = 2$ in Eqs. (7), and the solutions are given in Table II. As depicted in Figs. 3(a) and 3(f), the excitation profile for the S-PB3 sequence displays a wide flat top in the central region, while the width of the low excitation region becomes moderately small. This means that the obtained S-PB3 sequence not only makes selective excitation within a localized pulse area region, but also achieves population inversion with robustness against small pulse area error.

As long as the pulse number exceeds three, we can design various shapes for the excitation

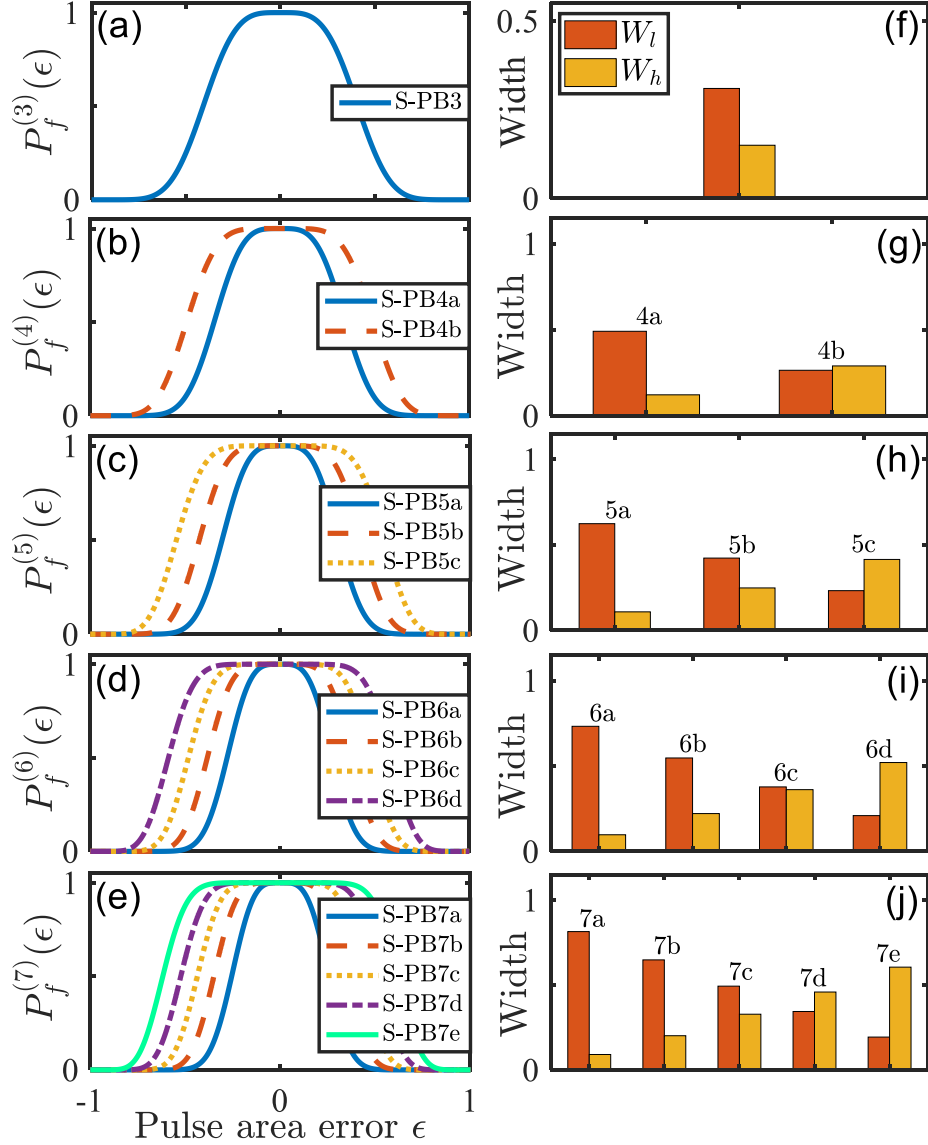


FIG. 3: Excitation profiles (left column) and the corresponding widths W_l and W_h (right column) for the S-PB3, S-PB4X, S-PB5X, S-PB6X and S-PB7X sequences. All θ_n are presented in Table II.

profile in S-PBN sequences, i.e., different widths of the flat top and two low excitation bottoms. Here, based on the shape of the excitation profile, we further subdivide and relabel them as the S-PBNX sequences, where $X = a, b, c, \dots$ corresponds to $M'_P = 4, 6, 8, \dots, 2N - 4$ and $M_P = 2N - M'_P$ in Eqs. (7). Figures 3(b)-(e) show the excitation profiles for the S-PBNX sequences from $N = 4$ to $N = 7$. To quantify the robustness against the small error, we define the width of the high excitation region $[P_f^{(N)}(\epsilon) \geq 0.999]$, which reads

$$W_h = |\epsilon_h^+ - \epsilon_h^-|, \quad (16)$$

TABLE II: Coupling strength ratios for the S-PBNX sequences (in units of π).

	θ_1	θ_2	θ_3	θ_4	θ_5	θ_6	θ_7
S-PB3	0.5537	1.4910	1.7227	–	–	–	–
S-PB4a	1.9842	0.0475	0.0238	1.7104	–	–	–
S-PB4b	0.9036	0.6474	0.4615	0.4677	–	–	–
S-PB5a	0.1409	1.9082	1.5695	0.4220	0.8698	–	–
S-PB5b	0.0835	0.0770	1.5016	1.1888	1.9306	–	–
S-PB5c	1.7192	0.2221	0.8691	0.0492	1.9330	–	–
S-PB6a	0.2738	0.4828	1.3861	1.4450	1.8460	1.3281	–
S-PB6b	1.9064	1.9160	0.3679	0.0166	1.1768	1.2686	–
S-PB6c	1.9305	1.6977	1.4651	1.4409	1.5025	1.5095	–
S-PB6d	0.1531	0.1932	1.3768	1.5882	0.3105	1.8089	–
S-PB7a	0.9832	1.0867	0.7896	1.3600	1.1954	1.7292	1.4578
S-PB7b	0.5937	1.1840	0.6068	0.2113	0.4956	0.5423	0.4916
S-PB7c	0.9369	1.1978	0.9863	1.3774	0.5201	0.3942	0.7759
S-PB7d	0.3728	1.6973	0.1163	1.4978	0.9549	1.6558	1.6569
S-PB7e	1.9388	1.7566	0.2566	0.8841	0.1531	1.7732	0.3155

where ϵ_h^+ and ϵ_h^- are two solutions satisfying $P_f^{(N)}(\epsilon) = 0.999$. In Figs. 3(g)-(j), W_l and W_h are displayed for different types of S-PBNX sequences. For a certain type, e.g., the type ‘a’, with the pulse number N increasing, the low excitation width gradually enlarges in their excitation profiles. For the same pulse number, different types of sequences have different W_l and W_h . Therefore, by solving different subequations in Eqs. (7), we can make the system only excited within a specific pulse area region.

B. Phase modulation

Next, we construct the NB and PB sequences by using the phase modulation in which ϕ_n and φ_n are recognized as the modulation parameters. For simplicity, the coupling strength ratio is fixed as $\theta_n = \pi/4$, i.e., $\Omega_n = \lambda_n$. In this situation, the CP sequence must be combined by odd pulses, because the system would return to the initial state when pulses are even. Besides, the phases of the first pulse can be arbitrary, since they do not affect population

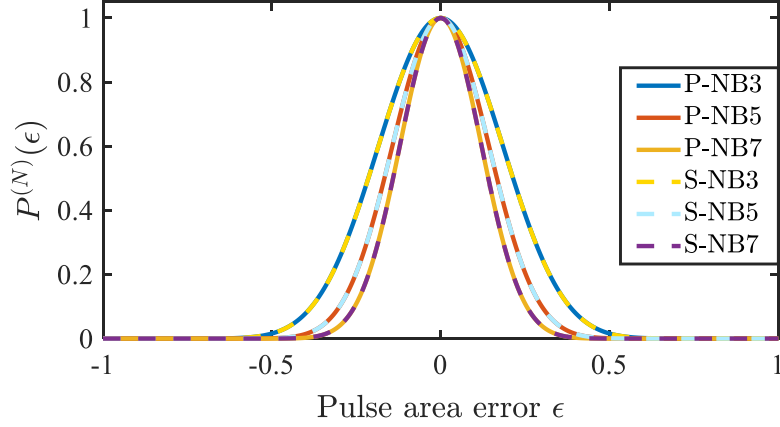


FIG. 4: Excitation profiles for the P-NBN and S-NBN sequences. The modulation parameters can be found in either Table I or III.

TABLE III: Phases for the P-NBN sequences (in units of π).

	P-NB3	P-NB5	P-NB7
ϕ_2	1.0000	0.8890	1.2301
φ_2	1.3333	1.2884	0.7066
ϕ_3	1.6667	1.0475	0.7358
φ_3	0.3333	0.0787	1.1614
ϕ_4	–	0.2278	1.4494
φ_4	–	0.9377	0.3906
ϕ_5	–	1.6684	0.0099
φ_5	–	1.2184	1.6341
ϕ_6	–	–	0.8954
φ_6	–	–	1.3972
ϕ_7	–	–	1.6944
φ_7	–	–	0.4215

transfer [39]. Thus, we simply set $\phi_1 = \varphi_1 = 0$. Similar to the strength modulation, we term the NB sequence with N pulses as the P-NBN sequence.

The target propagator of the N -pulse sequence in the absence of errors reads (up to a

global phase)

$$U^{(N)} = \begin{bmatrix} 0 & e^{-i \sum_{n=1}^N (-1)^n \Psi_n} & 0 \\ e^{i \sum_{n=1}^N (-1)^n \Psi_n} & 0 & 0 \\ 0 & 0 & 1 \end{bmatrix}, \quad (17)$$

where $\Psi_n = \phi_n - \varphi_n$ represents the phase difference in each pulse. We readily find from Eq. (17) that the transition probability of the target state $|f\rangle$ automatically reaches unity. Therefore, the total $2(N - 1)$ phases for the P-NBN sequence can be obtained by solving Eqs. (6) with $M_N = 4N - 2$, and the numerical solutions are given in Table III. Figure 4 shows the excitation profiles for the pulse number $N = 3, 5$ and 7 . For a comparison, the P-NBN sequences are also plotted in Fig. 4. We can see that the P-NBN and S-NBN sequences create almost identical excitation profile under the same pulse number. The reason can be found as follows. In the phase modulation, the transition probability is accurate up to the $(4N - 2)^{\text{th}}$ order for the P-NBN sequence. On the other hand, by the S-NBN sequence, all coefficients from $\tilde{x}_{N,2N+2}$ to $\tilde{x}_{N,4N-2}$ are extremely low and can be approximately regarded as nullification. As a result, both P-NBN and S-NBN sequences can almost eliminate the same number of error terms in Eqs. (6) and (7).

It is worth mentioning that there are no solutions for the P-PB3 sequence by solving Eqs. (7) with $M_P = 6$ and $M'_P = 4$. According to Eq. (8b), we can find a substituted solution by minimizing the following cost function

$$\mathcal{F}_{\text{PB}}^{(3)} = e^{-2}|x_{3,2}| + e^{-4}(|x_{3,4}| + |\tilde{x}_{3,4}|) + e^{-6}|\tilde{x}_{3,6}| \quad (18)$$

with the corresponding weight factor e^{-m} , and the numerical solution of phases for the P-PB3 sequence are presented in Table IV. It is observed in Fig. 5(a) that even though the substituted solution of the phases cannot fulfill Eqs. (7), the excitation profile for the P-PB3 sequence still exhibits a desired central flat top and bilateral flat bottoms. Moreover, the high and low excitation widths are similar to those in the excitation profile for the S-PB3 sequences.

When the pulse number $N > 3$, there are also various types of P-PBN sequences. Similarly, according to the shape of the excitation profiles, we further call them the P-PBNX sequences, where X = a, b, c, \dots correspond to $M'_P = 4, 8, 12, \dots, 4N - 8$ and $M_P = 4N - 2 - M'_P$. We present the substituted solutions for the P-PB5X and P-PB7X sequences in Table IV, and display the excitation profiles in Figs. 5(b) and 5(c),

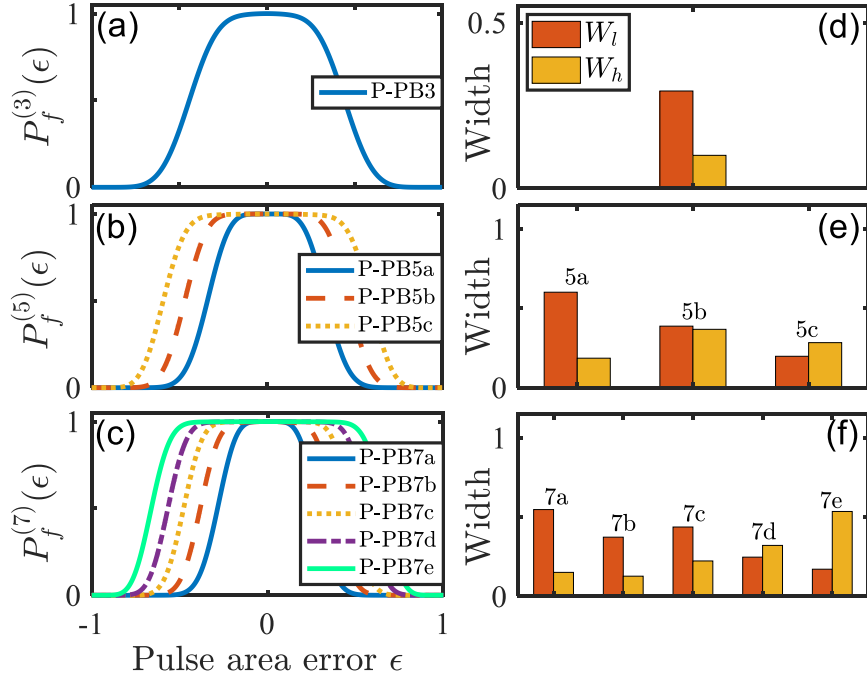


FIG. 5: Excitation profiles (left column) and the corresponding widths W_l and W_h (right column) for the P-PB3, P-PB5X and P-PB7X sequences. All ϕ_n and φ_n are presented in Table IV.

respectively. Compared to the S-PBNX sequence, the P-PBNX sequences also exhibit similar but not identical robustness and selectivity; see the slightly different W_l and W_h in Figs. 3(h), 3(j), 5(e) and 5(f). The reason is that, although the error coefficients are not entirely nullified in the P-PBNX sequences, they are suppressed to an extremely low level instead. Therefore, both modulation techniques are capable of obtaining the PB sequence with a desired excitation profile.

IV. ARBITRARY POPULATION TRANSFER BETWEEN TWO LOWER STATES

The construction method of NB and PB sequences is readily generalized to achieve arbitrary population transfer between two lower states in the three-state system. In the following, we make use of the pulse number $N = 5$ as examples to illustrate this issue. To make a distinction, we call the NB5 and PB5 sequences as the S_a -NB5 and S_a -PB5 sequences in the strength modulation, while label them as the P_a -NB5 and P_a -PB5X sequences in the phase modulation.

TABLE IV: Phases for the P-PB N X sequences (in units of π).

	PB3	PB5a	PB5b	PB5c	PB7a	PB7b	PB7c	PB7d	PB7e
ϕ_2	1.6631	1.3226	1.1066	0.5545	0.8918	1.0043	0.7689	0.0801	0.4857
φ_2	1.3708	1.9758	1.4412	0.6957	1.3931	1.4798	1.4526	0.6923	1.0137
ϕ_3	1.0588	0.1176	0.5884	1.2167	1.5376	1.5550	0.7495	0.1371	0.1068
φ_3	0.3485	0.9756	0.0506	1.6382	0.2099	1.0034	1.8600	1.9693	1.1928
ϕ_4	–	0.9860	1.0003	1.7003	0.5670	1.1009	1.3410	0.5222	1.9721
φ_4	–	1.0843	1.9541	1.1905	0.4894	1.9481	1.0660	0.9819	0.2282
ϕ_5	–	1.5012	0.2322	0.7557	1.2734	0.2563	1.5433	0.0705	0.7782
φ_5	–	1.9778	1.1589	1.5723	1.5472	1.5372	1.4520	1.5411	1.3012
ϕ_6	–	–	–	–	0.1126	1.8322	1.2466	1.5615	0.7032
φ_6	–	–	–	–	1.1991	0.2665	1.2015	1.9327	1.9502
ϕ_7	–	–	–	–	0.7005	1.9778	0.4884	0.5160	1.3763
φ_7	–	–	–	–	1.6726	1.1120	0.2337	0.7303	0.7019

TABLE V: Coefficients to be nullified for different types of sequences.

Sequence	Coefficients								
S _a -NB5	$\tilde{x}_{5,4}$	$\tilde{x}_{5,6}$	$y_{5,2}$	$\tilde{y}_{5,2}$					
S _a -PB5	$x_{5,2}$	$\tilde{x}_{5,4}$	$y_{5,2}$	$\tilde{y}_{5,2}$					
P _a -NB5	$\tilde{x}_{5,4}$	$\tilde{x}_{5,6}$	$\tilde{x}_{5,8}$	$\tilde{x}_{5,10}$	$y_{5,2}$	$y_{5,4}$	$\tilde{y}_{5,2}$	$\tilde{y}_{5,4}$	
P _a -PB5b	$x_{5,2}$	$x_{5,4}$	$\tilde{x}_{5,4}$	$\tilde{x}_{5,6}$	$y_{5,2}$	$y_{5,4}$	$\tilde{y}_{5,2}$	$\tilde{y}_{5,4}$	

First, Eq. (5) outlines the primary condition for achieving arbitrary population transfer. The design procedure is slightly distinct from those studied in Sec. III. Because part of modulation parameters are used to nullify the derivatives in the transition probability $P_e^{(N)}(\epsilon)$ according to Eq. (9), in the same pulse number, there are few types to the PB sequences for arbitrary population transfer. For instance, in the S_a-PB5 sequence, four coupling strength ratios are utilized to cancel out $y_{5,2}$, $\tilde{y}_{5,2}$, $x_{5,2}$, and $\tilde{x}_{5,4}$, resulting in a single type of the PB sequence. To make it more intuitive, we present in Table V all coefficients to be nullified for establishing the S_a-NB5, S_a-PB5, P_a-NB5, and P_a-PB5b sequences, where their solutions are given by Table VI.

TABLE VI: Coupling strength ratios and phases for the S_a -NB5, S_a -PB5, P_a -NB5, and P_a -PB5b sequences (in units of π).

\mathcal{P}	0.9	0.8	0.7	0.6	0.5	0.4	0.3	0.2	0.1
S_a -NB5									
θ_1	0.1216	1.1226	1.1233	1.1236	1.8763	0.8765	1.1227	0.8788	0.1174
θ_2	1.7835	0.7679	0.7543	0.7410	0.2726	1.2876	0.6951	1.3270	1.6390
θ_3	1.1930	0.1478	0.1096	0.0738	0.9620	1.9996	1.9586	0.0918	0.8365
θ_4	1.9769	0.9344	0.8987	0.8656	0.1673	1.2015	0.7609	1.2839	1.6533
θ_5	0.6446	1.6080	1.5779	1.5502	1.4766	0.5039	1.4669	0.5665	0.3896
S_a -PB5									
θ_1	1.2200	1.2324	1.7581	1.7499	0.2577	1.2650	0.2725	1.2808	0.9936
θ_2	1.6545	1.7206	1.2290	1.1850	0.8562	1.8972	0.9403	1.9897	0.9936
θ_3	0.9604	1.0559	1.8707	1.8065	0.2536	1.3130	0.3750	1.4447	1.0320
θ_4	0.1420	0.2114	0.7332	0.6835	1.3639	0.4115	1.4617	0.5189	1.0320
θ_5	0.4173	0.4674	0.4912	0.4532	1.5839	0.6217	1.6623	0.7093	0.0512
P_a -NB5									
θ	0.8424	1.8321	1.1578	0.8281	1.1242	1.0925	1.8988	1.8778	0.0285
ϕ_2	1.4751	1.2427	0.6861	1.0835	1.3505	0.7847	1.3257	1.3005	0.8716
φ_2	0.1375	0.9586	1.0145	1.9725	0.8904	1.0196	0.1656	0.9449	1.1301
ϕ_3	1.3655	0.5775	1.1615	1.9709	0.5951	1.3670	1.8897	0.7344	1.3311
φ_3	1.1045	1.7474	0.1907	0.9366	1.9091	0.2470	1.1773	1.8017	0.7655
ϕ_4	0.5345	1.0085	1.3687	0.5786	0.6205	0.7631	0.8998	0.5405	1.8695
φ_4	0.2872	1.8213	1.9197	0.8735	0.1019	0.1208	0.5262	1.5857	0.1531
ϕ_5	0.6323	1.9165	0.1921	1.2124	1.5372	1.8727	0.6552	1.6259	0.6640
φ_5	1.0487	1.0543	1.0879	1.9511	1.2865	0.9275	1.5082	0.4730	1.3318
P_a -PB5b									
θ	0.1988	1.8236	0.8423	1.1410	1.8780	1.8910	0.0923	0.1194	0.9821
ϕ_2	0.7756	1.2414	0.6145	1.4103	0.2878	0.2254	1.3906	1.3457	0.4795
φ_2	0.7756	1.2395	0.6145	1.4103	1.7025	0.2254	1.3906	0.5910	1.7838
ϕ_3	1.1354	0.8789	1.0493	0.9612	0.9553	0.9285	0.9585	0.6404	1.0012
φ_3	0.0731	1.9549	1.7835	0.2469	0.8287	1.3337	0.2075	1.4067	1.2750
ϕ_4	1.5089	0.5249	1.2708	0.7553	1.6212	0.9666	0.7334	0.5750	1.8134
φ_4	0.4466	1.5980	0.0050	0.0411	1.1949	1.3717	1.9824	1.3433	0.9507
ϕ_5	0.2770	1.7618	1.9905	0.0459	0.9992	1.5673	0.0218	1.5403	1.1453
φ_5	1.6150	0.4147	1.1533	0.8822	0.0413	0.5503	0.7901	0.2147	0.1682

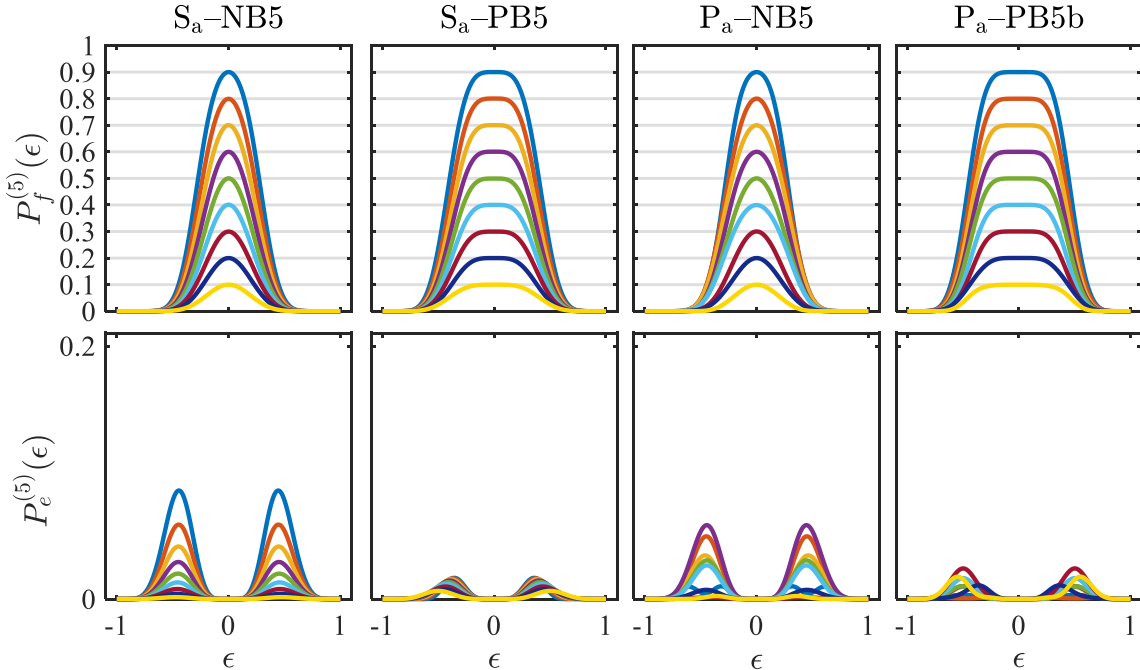


FIG. 6: Excitation profiles for the states $|f\rangle$ (top panels) and $|e\rangle$ (bottom panels) in the S_a-NB5, S_a-PB5, P_a-NB5, and P_a-PB5b sequences. All modulation parameters are presented in Table VI.

In Figs. 6(a)-(d), we plot different excitation profiles of the target state $|f\rangle$ for the S_a-NB5, S_a-PB5, P_a-NB5, and P_a-PB5b sequences, respectively, while the corresponding population of the third state $|e\rangle$ are presented in Figs. 6(e)-(h). As expected, Figs. 6(a)-(d) verify that the current design is successful in achieving arbitrary population transfer for different types of NB and PB sequences. Moreover, Figs. 6(e)-(h) demonstrate the current sequences have remarkable ability for suppressing leakage, because the population of the excited state is always restricted at an extremely low level for all ϵ .

V. INFLUENCE OF IMPERFECT PULSES

This section examines the effectiveness of the current sequences when the pulses are imperfect. Imperfect pulses, such as waveform distortion and phase or detuning offset, are usually caused by defective experimental devices, imprecise operations, external noises, etc. In the following, we use the S-NB5 and P-NB5 sequences to investigate the impact of imperfect pulses.

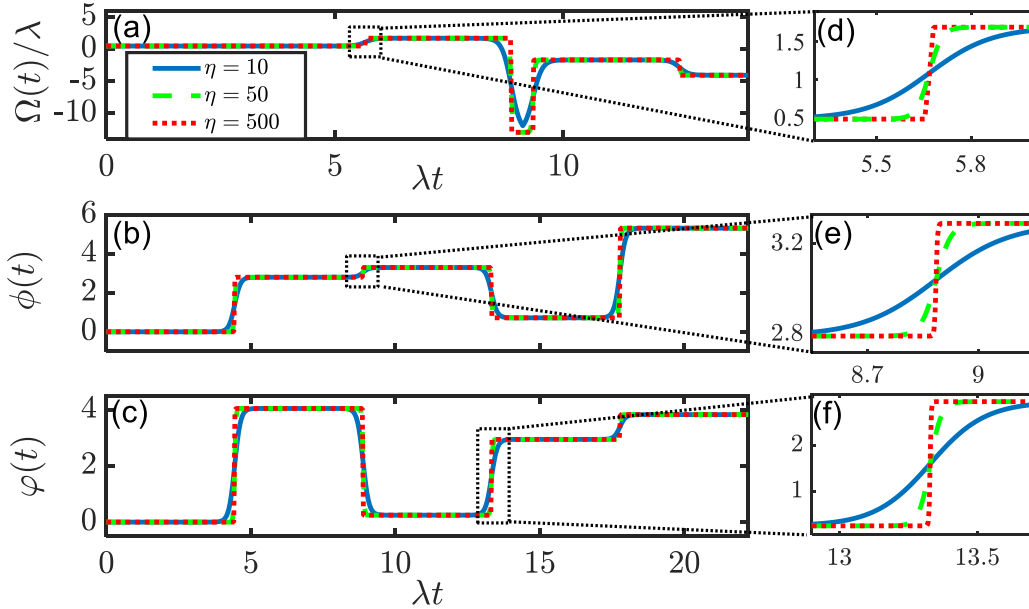


FIG. 7: Different waveforms of the function $\alpha(t)$. Top: the coupling strength $\Omega(t)$. Middle: the phase $\phi(t)$. Bottom: the phase $\varphi(t)$.

A. Waveform distortion

In reality, due to the inability of instantaneously switching between different values, the unknown rising and falling edges inevitably appear in the square wave. To visualize the influence of waveform distortion on the performance of the transition probability, we utilize a time-dependent function to simulate the square wave, whose form is expressed as

$$\alpha(t) = \frac{\alpha_n - \alpha_{n-1}}{1 + \exp\left[\eta\left(t - \sum_{l=1}^{n-1} t_l\right)\right]}, \quad \tau_{n-2} < t \leq \tau_{n-1}, \quad (19)$$

with

$$\tau_0 = 0, \quad \tau_k = \sum_{l=1}^k t_l + \frac{t_{k+1}}{2}, \quad \tau_4 = T, \quad k = 1, 2, 3,$$

where η is a dimensionless parameter for controlling the magnitude of the rising and falling edges. Here, $\alpha(t)$ denotes the expression of the coupling strength $\Omega(t)$ in the strength modulation, while represents $\phi(t)$ and $\varphi(t)$ in the phase modulation. We plot in Figs. 7(a)-(c) the waveforms of $\alpha(t)$ with different η . It is shown in Figs. 7(d)-(f) that the function $\alpha(t)$ gets closer to a perfect square wave as the parameter η increases. For example, the function $\alpha(t)$ can be almost regarded as the square wave at $\eta = 500$. Note that the function $\alpha(t)$

becomes a smooth curve when η is small meaning that there is severe waveform distortion in the square wave.

As shown in Figs. 8(a) and 8(b), the S-NB5 sequence possesses a well performance even in the presence of severe waveform distortion ($\eta \sim 10$), but the effectiveness of the P-NB5 sequence highly depends on the waveform. Applying a near-perfect square waveform ($\eta \sim 100$) can greatly protect the selectivity of the P-NB5 sequence from the pulse area error. The reason is that the phase modulation relies heavily on high-precision phases so as to ensure the operational accuracy [76].

B. Phase errors

Previous studies [31, 76] have demonstrated that the effectiveness of the CP design may be hindered by phase errors. It becomes particularly obvious in the phase modulation, since the accuracy of phases directly impacts the waveform of sequences [77]. Therefore, it is imperative to evaluate the validity of the current method when the phases are inaccurate.

In the strength modulation, the phase error is assumed to exhibit in the phase difference Ψ_n of each pulse, i.e.,

$$\Psi_n \rightarrow \Psi_n(1 + \delta_\Psi), \quad (20)$$

while it appears in ϕ_n and φ_n in the phase modulation,

$$\phi_n \rightarrow \phi_n(1 + \delta_\phi), \quad \varphi_n \rightarrow \varphi_n(1 + \delta_\varphi). \quad (21)$$

Figures 8(c) and 8(d) demonstrate the transition probability of the state $|f\rangle$ as a function of the pulse area error and the phase error for the S-NB5 and P-NB5 sequences, respectively, where we set $\delta_\phi = \delta_\varphi = \delta_{\phi\varphi}$ for simplicity. A very striking feature in Fig. 8(c) is that the phase error does not impact the excitation profile in the strength modulation. This is due to the fact that phase errors become global when the phase difference Ψ_n is the same for each pulse. As a result, the S-NB sequence is inherently robust against phase errors. In regards to the phase modulation, the high excitation region experiences a slight change, as illustrated by the orange region in Fig. 8(d). The reason is that the inaccurate phases do not satisfy Eqs. (6) any more, resulting in the low-order error coefficients not being fully eliminated. Therefore, when the system exhibits phase errors, the strength modulation outperforms the phase modulation.

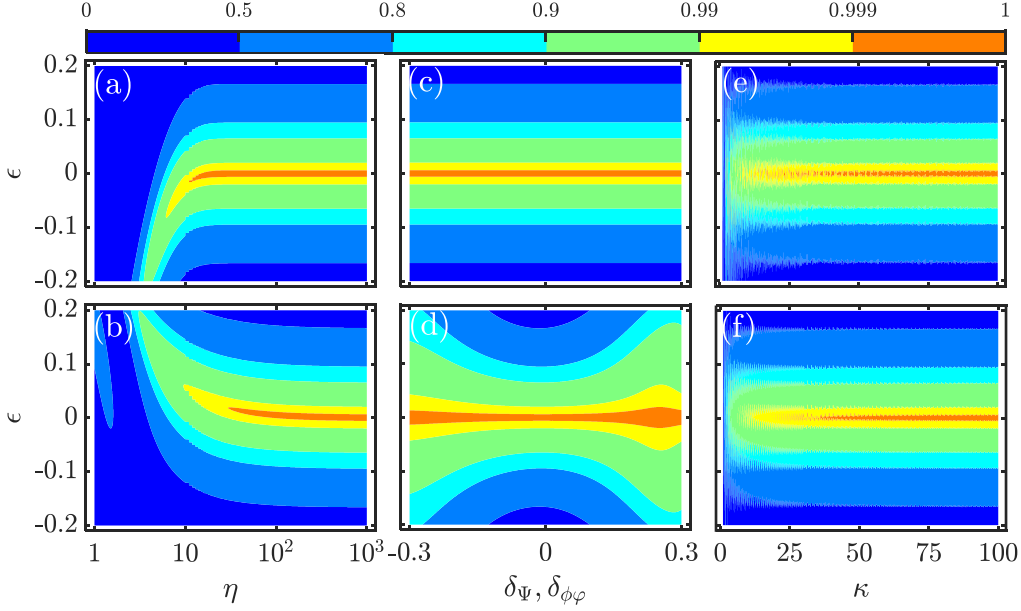


FIG. 8: Excitation profiles in the presence of different types of errors. Left column: $P_f^{(5)}(\epsilon, \eta)$ vs ϵ and η . Middle column: $P_f^{(5)}(\epsilon, \delta_{\Psi/\phi\phi})$ vs ϵ and $\delta_{\Psi/\phi\phi}$. Right column: $P_f^{(5)}(\epsilon, \omega_f)$ vs ϵ and κ . The top and bottom rows denote the S-NB5 and P-NB5 sequences, respectively. Here, $\eta = 1000$ in panels (c)-(f), $\omega_g = 1.2\omega_f$ in panels (e) and (f), and other parameters can be found in Tables I and III.

C. Effectiveness beyond RWA

In some quantum systems, such as superconducting circuits [78], the ultra-strong coupling regime is possible to attain under the state-of-art technology [79, 80]. Namely, the coupling strength is comparable to the transition frequency. In this situation, the counter-rotating terms ignored in RWA can have a notable effect on the dynamics. Next, we investigate the effectiveness of the pulse sequences beyond RWA.

To this end, we retain the counter-rotating terms in Hamiltonian (2). We use a dimensionless parameter κ to denote the ratio of the frequency ω_f and the coupling strength λ , which reads $\kappa = \omega_f/\lambda$. Obviously, a large κ means that the transition frequency is far large than the coupling strength so that the RWA can be justified. In Figs. 8(e) and 8(f), we present the excitation profiles for the S-NB5 and P-NB5 sequences as a function of the error ϵ and the parameter κ . It can be observed that the excitation profiles for both sequences exhibit significant deformation at small κ ($\kappa < 5$), because the RWA cannot be satisfied,

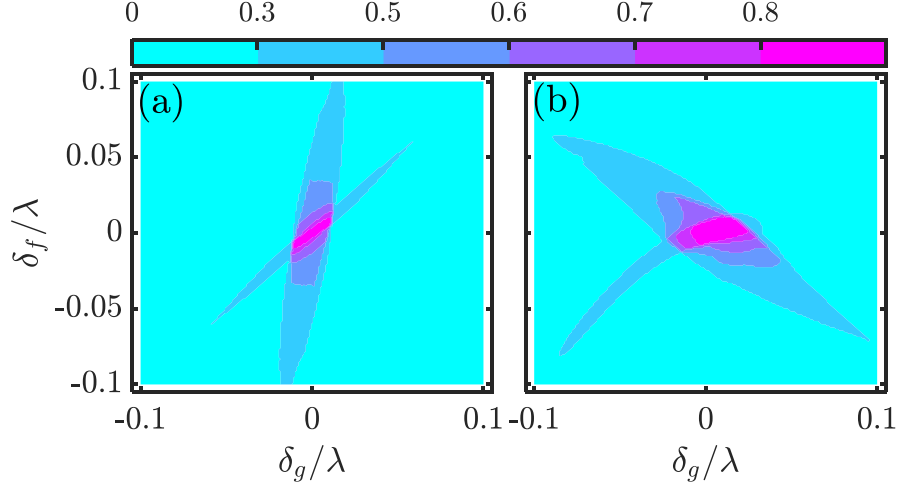


FIG. 9: Low excitation width W_l of the excitation profile for (a) S-NB5 and (b) P-NB5 sequences against the detunings δ_g and δ_f . All parameters can be found in Tables I and III.

leading to invalidness of the NB sequence. As the value of κ increases, both sequences perform well. And the phase modulation possesses better robustness to the influence caused by the counter-rotating terms. To be specific, the P-NB5 sequence becomes more capable of generating a narrow excitation profile at a moderate κ ($\kappa \sim 25$), while the S-NB5 sequence requires a higher κ ($\kappa > 40$) to achieve the same effectiveness. The reason is that, the coupling strengths in different sub-pulses are diverse from each other and thus cannot always be much smaller than the transition frequency in the strength modulation. In this situation, the unfavorable influence of the counter-rotating terms becomes obvious and is hard to be ignored.

D. Detuning errors

Detuning errors generally result from a discrepancy between the transition frequency and the driving field frequency, and make the pulses become off-resonance. In the following, we study the subject of $\delta_{g(f)} \neq 0$.

Figures 9(a) and 9(b) demonstrate the low excitation width W_l of the excitation profile for the S-NB5 and P-NB5 sequences at different δ_g and δ_f . The P-NB5 sequence exhibits better selectivity to excitation when a small detuning occurs, while it is not satisfactory for the S-NB5 sequence, as indicated by the pink regions in Figs. 9(a) and 9(b). These

results show that the strength modulation is sensitive to detuning errors in NB sequences. In the strength modulation, Ω varies in the whole sequence. Once the detuning is larger than the coupling strength, population transfer cannot be successfully manipulated due to the large detuning. As a consequence, the selective excitation for the NB sequence would be dramatically affected. On the other hand, in the phase modulation, the coupling strength consistently exceeds the detunings, making the selective excitation less affected.

VI. CONCLUSION

In summary, we propose a systematic method for constructing the NB and PB sequences that to implement efficient population inversion in the three-state system. The modulation parameters of sequences are designed through either nullifying the coefficients of error terms or minimizing the cost function. The former is typically preferred due to its ability to create a perfect excitation profile, with flatter top or bottoms. However, the latter offers greater universality as it can tackle the situation in which the former fails, and still successfully shape a nearly perfect excitation profile. The results shows that both the strength and phase modulations can produce the NB sequences with identical excitation profiles, and the PB sequences with the desired shape of excitation profiles.

Moreover, the current method can be also extended to create the NB and PB sequences for arbitrary population transfer. These sequences exhibit remarkable suppression of leakage to the excited state. It is very important that, the sequences are robust against waveform distortion by using the strength modulation, while perform well in off-resonance conditions by the phase modulation. Furthermore, the design method remains valid for both modulation techniques beyond RWA, where the phase modulation performs better. We hope this work can offer a promising candidate for precise quantum control (e.g., the high-precision addressing operation by laser fields) in different physical systems.

Acknowledgments

This work is supported by the Natural Science Foundation of Fujian Province under Grant No. 2021J01575, the Natural Science Funds for Distinguished Young Scholar of Fujian Province under Grant No. 2020J06011, and the Project from Fuzhou University under Grant

No. JG202001-2.

- [1] M. H. Levitt and R. Freeman, NMR population inversion using a composite pulse, *J. Magn. Reson.* **33**, 473 (1979).
- [2] S. Wimperis, Broadband and narrowband composite excitation sequences, *J. Magn. Reson.* **86**, 46 (1990).
- [3] S. Wimperis, Composite pulses with rectangular excitation and inversion profiles, *J. Magn. Reson.* **83**, 509 (1989).
- [4] R. Tycko, H. Cho, E. Schneider, and A. Pines, Composite pulses without phase distortion, *J. Magn. Reson.* **61**, 90 (1985).
- [5] M. H. Levitt, Composite pulses, *Prog. NMR Spectrosc.* **18**, 61 (1986).
- [6] B. T. Torosov and N. V. Vitanov, Experimental Demonstration of Composite Pulses on IBM's Quantum Computer, *Phys. Rev. Appl.* **18**, 034062 (2022).
- [7] S. S. Ivanov, B. T. Torosov, and N. V. Vitanov, High-Fidelity Quantum Control by Polychromatic Pulse Trains, *Phys. Rev. Lett.* **129**, 240505 (2022).
- [8] H. L. Gevorgyan and N. V. Vitanov, Deterministic generation of arbitrary ultrasmall excitation of quantum systems by composite pulse sequences, *Phys. Rev. A* **108**, 032614 (2023).
- [9] T. Peters, S. S. Ivanov, D. Englisch, A. A. Rangelov, N. V. Vitanov, and T. Halfmann, Variable ultrabroadband and narrowband composite polarization retarders, *Appl. Opt.* **51**, 7466 (2012).
- [10] C. Counsell, M. Levitt, and R. Ernst, Analytical theory of composite pulses, *J. Magn. Reson.* **63**, 133 (1985).
- [11] S. Wimperis, Iterative schemes for phase-distortionless composite 180° pulses, *J. Magn. Reson.* **93**, 199 (1991).
- [12] J. A. Jones, Quantum computing with NMR, *Prog. NMR Spectrosc.* **59**, 91 (2011).
- [13] S. Odedra and S. Wimperis, Use of composite refocusing pulses to form spin echoes, *J. Magn. Reson.* **214**, 68 (2012).
- [14] S. Odedra, M. J. Thrippleton, and S. Wimperis, Dual-compensated antisymmetric composite refocusing pulses for NMR, *J. Magn. Reson.* **225**, 81 (2012).
- [15] K. R. Brown, A. W. Harrow, and I. L. Chuang, Arbitrarily accurate composite pulse

- sequences, *Phys. Rev. A* **70**, 052318 (2004).
- [16] H. K. Cummins and J. A. Jones, Use of composite rotations to correct systematic errors in NMR quantum computation, *New J. Phys.* **2**, 006 (2000).
- [17] R. S. Said and J. Twamley, Robust control of entanglement in a nitrogen-vacancy center coupled to a ^{13}C nuclear spin in diamond, *Phys. Rev. A* **80**, 032303 (2009).
- [18] C. Kabytayev, T. J. Green, K. Khodjasteh, M. J. Biercuk, L. Viola, and K. R. Brown, Robustness of composite pulses to time-dependent control noise, *Phys. Rev. A* **90**, 012316 (2014).
- [19] A. Dunning, R. Gregory, J. Bateman, N. Cooper, M. Himsworth, J. A. Jones, and T. Freegerde, Composite pulses for interferometry in a thermal cold atom cloud, *Phys. Rev. A* **90**, 033608 (2014).
- [20] G. Demeter, Composite pulses for high-fidelity population inversion in optically dense, inhomogeneously broadened atomic ensembles, *Phys. Rev. A* **93**, 023830 (2016).
- [21] B. T. Torosov and N. V. Vitanov, Composite stimulated Raman adiabatic passage, *Phys. Rev. A* **87**, 043418 (2013).
- [22] F.-Q. Dou, H. Cao, J. Liu, and L.-B. Fu, High-fidelity composite adiabatic passage in nonlinear two-level systems, *Phys. Rev. A* **93**, 043419 (2016).
- [23] M. Al-Mahmoud, V. Coda, A. Rangelov, and G. Montemezzani, Broadband polarization rotator with tunable rotation angle composed of three wave plates, *Phys. Rev. Appl.* **13**, 014048 (2020).
- [24] T. Zanon-Willette, D. Wilkowski, R. Lefevre, A. V. Taichenachev, and V. I. Yudin, Generalized hyper-Ramsey-Bordé matter-wave interferometry: Quantum engineering of robust atomic sensors with composite pulses, *Phys. Rev. Research* **4**, 023222 (2022).
- [25] S. Bodenstedt, M. W. Mitchell, and M. C. D. Tayler, Meridional composite pulses for low-field magnetic resonance, *Phys. Rev. A* **106**, 033102 (2022).
- [26] J. Zhou, S. Li, G.-Z. Pan, G. Zhang, T. Chen, and Z.-Y. Xue, Nonadiabatic geometric quantum gates that are insensitive to qubit-frequency drifts, *Phys. Rev. A* **103**, 032609 (2021).
- [27] T. Chen and Z.-Y. Xue, Nonadiabatic geometric quantum computation with parametrically tunable coupling, *Phys. Rev. Appl.* **10**, 054051 (2018).
- [28] G. Dridi, M. Mejatty, S. J. Glaser, and D. Sugny, Robust control of a NOT gate by composite pulses, *Phys. Rev. A* **101**, 012321 (2020).

- [29] H. L. Gevorgyan and N. V. Vitanov, Ultrahigh-fidelity composite rotational quantum gates, [Phys. Rev. A **104**, 012609 \(2021\)](#).
- [30] Y. Ota and Y. Kondo, Composite pulses in NMR as nonadiabatic geometric quantum gates, [Phys. Rev. A **80**, 024302 \(2009\)](#).
- [31] Z.-C. Shi, C. Zhang, D. Ran, Y. Xia, R. Ianculescu, A. Friedman, X. X. Yi, and S.-B. Zheng, Composite pulses for high fidelity population transfer in three-level systems, [New J. Phys. **24**, 023014 \(2022\)](#).
- [32] H. Xu, X.-K. Song, D. Wang, and L. Ye, Robust coherent control in three-level quantum systems using composite pulses, [Opt. Express **30**, 3125 \(2022\)](#).
- [33] L. M. K. Vandersypen and I. L. Chuang, NMR techniques for quantum control and computation, [Rev. Mod. Phys. **76**, 1037 \(2005\)](#).
- [34] J. A. Jones, Designing short robust NOT gates for quantum computation, [Phys. Rev. A **87**, 052317 \(2013\)](#).
- [35] B. T. Torosov, S. Guérin, and N. V. Vitanov, High-fidelity adiabatic passage by composite sequences of chirped pulses, [Phys. Rev. Lett. **106**, 233001 \(2011\)](#).
- [36] G. T. Genov, D. Schraft, T. Halfmann, and N. V. Vitanov, Correction of arbitrary field errors in population inversion of quantum systems by universal composite pulses, [Phys. Rev. Lett. **113**, 043001 \(2014\)](#).
- [37] G. H. Low, T. J. Yoder, and I. L. Chuang, Optimal arbitrarily accurate composite pulse sequences, [Phys. Rev. A **89**, 022341 \(2014\)](#).
- [38] J. A. Jones, Robust Ising gates for practical quantum computation, [Phys. Rev. A **67**, 012317 \(2003\)](#).
- [39] B. T. Torosov and N. V. Vitanov, Arbitrarily accurate variable rotations on the Bloch sphere by composite pulse sequences, [Phys. Rev. A **99**, 013402 \(2019\)](#).
- [40] H.-N. Wu, C. Zhang, J. Song, Y. Xia, and Z.-C. Shi, Composite pulses for optimal robust control in two-level systems, [Phys. Rev. A **107**, 023103 \(2023\)](#).
- [41] S. Kukita, H. Kiya, and Y. Kondo, General off-resonance-error-robust symmetric composite pulses with three elementary operations, [Phys. Rev. A **106**, 042613 \(2022\)](#).
- [42] C. Zhang, Y. Liu, Z.-C. Shi, J. Song, Y. Xia, and S.-B. Zheng, Robust population inversion in three-level systems by composite pulses, [Phys. Rev. A **105**, 042414 \(2022\)](#).
- [43] H. K. Cummins, G. Llewellyn, and J. A. Jones, Tackling systematic errors in quantum logic

- gates with composite rotations, *Phys. Rev. A* **67**, 042308 (2003).
- [44] S. S. Ivanov and N. V. Vitanov, Composite two-qubit gates, *Phys. Rev. A* **92**, 022333 (2015).
- [45] T. Ichikawa, M. Bando, Y. Kondo, and M. Nakahara, Designing robust unitary gates: application to concatenated composite pulses, *Phys. Rev. A* **84**, 062311 (2011).
- [46] I. Cohen, A. Rotem, and A. Retzker, Refocusing two-qubit-gate noise for trapped ions by composite pulses, *Phys. Rev. A* **93**, 032340 (2016).
- [47] B. T. Torosov and N. V. Vitanov, High-fidelity error-resilient composite phase gates, *Phys. Rev. A* **90**, 012341 (2014).
- [48] E. Mount, C. Kabytayev, S. Crain, R. Harper, S.-Y. Baek, G. Vrijsen, S. T. Flammia, K. R. Brown, P. Maunz, and J. Kim, Error compensation of single-qubit gates in a surface-electrode ion trap using composite pulses, *Phys. Rev. A* **92**, 060301(R) (2015).
- [49] B. T. Torosov and N. V. Vitanov, High-fidelity composite quantum gates for Raman qubits, *Phys. Rev. Research* **2**, 043194 (2020).
- [50] Z.-C. Shi, H.-N. Wu, L.-T. Shen, J. Song, Y. Xia, X. X. Yi, and S.-B. Zheng, Robust single-qubit gates by composite pulses in three-level systems, *Phys. Rev. A* **103**, 052612 (2021).
- [51] L. Xiao and J. A. Jones, Robust logic gates and realistic quantum computation, *Phys. Rev. A* **73**, 032334 (2006).
- [52] H. Häffner, C. Roos, and R. Blatt, Quantum computing with trapped ions, *Phys. Rep.* **469**, 155 (2008).
- [53] J. Joo, Y. L. Lim, A. Beige, and P. L. Knight, Single-qubit rotations in two-dimensional optical lattices with multiqubit addressing, *Phys. Rev. A* **74**, 042344 (2006).
- [54] L. J. LeBlanc and J. H. Thywissen, Species-specific optical lattices, *Phys. Rev. A* **75**, 053612 (2007).
- [55] J. Cho, Addressing Individual Atoms in Optical Lattices with Standing-Wave Driving Fields, *Phys. Rev. Lett.* **99**, 020502 (2007).
- [56] R. Tycko and A. Pines, Iterative schemes for broad-band and narrow-band population inversion in NMR, *Chem. Phys. Lett.* **111**, 462 (1984).
- [57] S. S. Ivanov and N. V. Vitanov, High-fidelity local addressing of trapped ions and atoms by composite sequences of laser pulses, *Opt. Lett.* **36**, 1275 (2011).
- [58] A. Shaka and R. Freeman, Spatially selective radiofrequency pulses, *J. Magn. Reson.* **59**, 169 (1984).

- [59] B. T. Torosov, S. S. Ivanov, and N. V. Vitanov, Narrowband and passband composite pulses for variable rotations, *Phys. Rev. A* **102**, 013105 (2020).
- [60] N. V. Vitanov, Arbitrarily accurate narrowband composite pulse sequences, *Phys. Rev. A* **84**, 065404 (2011).
- [61] B. T. Torosov and N. V. Vitanov, Narrowband composite two-qubit gates for crosstalk suppression, *Phys. Rev. A* **107**, 032618 (2023).
- [62] B. T. Torosov and N. V. Vitanov, Smooth composite pulses for high-fidelity quantum information processing, *Phys. Rev. A* **83**, 053420 (2011).
- [63] E. Kyoseva and N. V. Vitanov, Arbitrarily accurate passband composite pulses for dynamical suppression of amplitude noise, *Phys. Rev. A* **88**, 063410 (2013).
- [64] H. M. Cho, R. Tycko, A. Pines, and J. Guckenheimer, Iterative maps for bistable excitation of two-level systems, *Phys. Rev. Lett.* **56**, 1905 (1986).
- [65] J. T. Merrill, S. C. Doret, G. Vittorini, J. P. Addison, and K. R. Brown, Transformed composite sequences for improved qubit addressing, *Phys. Rev. A* **90**, 040301(R) (2014).
- [66] G. T. Genov, B. T. Torosov, and N. V. Vitanov, Optimized control of multistate quantum systems by composite pulse sequences, *Phys. Rev. A* **84**, 063413 (2011).
- [67] S. Husain, M. Kawamura, and J. A. Jones, Further analysis of some symmetric and antisymmetric composite pulses for tackling pulse strength errors, *J. Magn. Reson.* **230**, 145 (2013).
- [68] J. R. Morris and B. W. Shore, Reduction of degenerate two-level excitation to independent two-state systems, *Phys. Rev. A* **27**, 906 (1983).
- [69] E. Majorana, Atomi orientati in campo magnetico variabile, *Nuovo Cimento* **9**, 43 (1932).
- [70] Y.-C. Zhang, X.-F. Zhou, X. Zhou, G.-C. Guo, and Z.-W. Zhou, Cavity-Assisted Single-Mode and Two-Mode Spin-Squeezed States via Phase-Locked Atom-Photon Coupling, *Phys. Rev. Lett.* **118**, 083604 (2017).
- [71] M. Wollenhaupt, V. Engel, and T. Baumert, Femtosecond laser photoelectron spectroscopy on atoms and small molecules: Prototype studies in quantum control, *Annu. Rev. Phys. Chem.* **56**, 25 (2005).
- [72] J. Cho, D. G. Angelakis, and S. Bose, Fractional Quantum Hall State in Coupled Cavities, *Phys. Rev. Lett.* **101**, 246809 (2008).
- [73] C. Ye, Q. Zhang, Y.-Y. Chen, and Y. Li, Effective two-level models for highly efficient inner-

- state enantioseparation based on cyclic three-level systems of chiral molecules, *Phys. Rev. A* **100**, 043403 (2019).
- [74] J. P. Kestner, X. Wang, L. S. Bishop, E. Barnes, and S. Das Sarma, Noise-resistant control for a spin qubit array, *Phys. Rev. Lett.* **110**, 140502 (2013).
- [75] J. Ghosh, S. N. Coppersmith, and M. Friesen, Pulse sequences for suppressing leakage in single-qubit gate operations, *Phys. Rev. B* **95**, 241307(R) (2017).
- [76] B. T. Torosov, B. W. Shore, and N. V. Vitanov, Coherent control techniques for two-state quantum systems: a comparative study, *Phys. Rev. A* **103**, 033110 (2021).
- [77] B. T. Torosov and N. V. Vitanov, Composite pulses with errant phases, *Phys. Rev. A* **100**, 023410 (2019).
- [78] Z.-L. Xiang, S. Ashhab, J. Q. You, and F. Nori, Hybrid quantum circuits: Superconducting circuits interacting with other quantum systems, *Rev. Mod. Phys.* **85**, 623 (2013).
- [79] T. Niemczyk, F. Deppe, H. Huebl, E. P. Menzel, F. Hocke, M. J. Schwarz, J. J. Garcia-Ripoll, D. Zueco, T. Hümmer, E. Solano, A. Marx, and R. Gross, Circuit quantum electrodynamics in the ultrastrong-coupling regime, *Nat. Phys.* **6**, 772 (2010).
- [80] T. Jaako, J. J. García-Ripoll, and P. Rabl, Ultrastrong-coupling circuit QED in the radio-frequency regime, *Phys. Rev. A* **100**, 043815 (2019).